Contents lists available at ScienceDirect

Materials Research Bulletin

Enhanced photocatalytic degradation of phenol over Ag_3PO_4-$BiOCl_{1-x}Br_x$ composites

Yi Ling Qi[a], Gui Han[a,*], Xu Chun Song[b,*]

[a] School of Chemistry and Chemcal Engineering, Yangzhou University, Yangzhou, 225002, PR China
[b] Department of Chemistry, Fujian Normal University, Fuzhou, 350007, PR China

A R T I C L E   I N F O

A B S T R A C T

In this paper, a series of Ag_3PO_4-$BiOCl_{1-x}Br_x$ composites with adjustable band gap has been fabricated by using a facile two-step synthetic method. The photocatalytic activity of Ag_3PO_4-$BiOCl_{1-x}Br_x$ was evaluated by photocatalytic decomposition of phenol aqueous solution under simulated solar light irradiation. The result shows that Ag_3PO_4-$BiOCl_{0.75}Br_{0.25}$ (1:5) composite possesses the best photocatalytic activity among all the as-prepared samples. The photocatalytic activity of Ag_3PO_4-BiOCl can be enhanced mainly owing to the strong light absorption ability by loading Ag_3PO_4 on the surface of BiOCl, while the photocatalytic activities of Ag_3PO_4-$BiOCl_{1-x}Br_x$ (x = 0.25, 0.5, 0.75 and 1) composites could be enhanced by restraining the recombination of photo-generated electron-hole pairs. The enhanced solar-light photocatalytic activities of Ag_3PO_4-$BiOCl_{1-x}Br_x$ composites could be ascribed to the adjustable energy band structure, which facilitates the separation of photoinduced carriers. In addition, superoxide radicals ($\cdot O_2^-$), holes (h^+) and $\cdot OH$ are considered to dominate the photocatalytic degration process. Moreover, a possible mechanism of deep understanding on the base of experimental results was proposed.

1. Introduction

The shortage of water resources has received extensive attention owing to its crucial role in the development of society and human health. The pollution of industrial has become a major problem owing to the increasing manufactured products and the precursor chemicals. Among the recalcitrant organic pollutants, phenol and its derivatives are the most recalcitrant organic compounds, and these pollutants are usually discharged from various chemical and pharmaceutical industries, polluting the environment and water resources [1–3]. If not treated properly, it will affect the aquatic life and finally might lead to a severe threat to human health. Therefore, various phenol-containing wastewater techniques were developed, such as biological treatments, catalytic oxidation, electrochemical, advanced oxidation processes and so on. Among these methods, photocatalysis as an effective technology has become a popular choice to convert organic pollutants into harmless products. It has been widely used for the degradation of phenol and phenolic pollutants in wastewater [4]. Many researchers are focusing on using solar light for the photodegradation of organic pollutants in wastewater. Silver orthophosphate (Ag_3PO_4) is widely regarded as a promising material owing to the excellent photocatalytic performance, excellent oxidative capacities, rich morphologies as well as the

photodegradation of organic dyes (e.g. Methylene blue, or Rhodamine B, etc.) under the solar irradiation [5–9]. Therefore, Ag_3PO_4 is being thoroughly researched by increasing researchers [10–13]. Unfortunately, the comparatively high recombination ratio of photogenerated carriers and the low structural stability limit its practical application.

Recently, as protuberant ternary oxide semiconductors of bismuth oxyhalides (BiOX, X = Cl, Br and I) have drawn extensive interests, because of the potential photocatalytic abilities under UV and solar light irradiation [14–16]. BiOX also represents better photocatalytic activity than Ag_3PO_4 for the existence of layers of $[Bi_2O_2]^{2+}$ interleaved through double layer of halogen atoms (X = Cl, Br and I) in the BiOX [17]. The internal electric field formed between the positive layers $[Bi_2O_2]^{2+}$ and anionic halogen, which is beneficial to the efficient separation of electron-hole pairs. However, BiOCl is only active at ultraviolet light due to the wide band gap, while BiOI and BiOBr show visible light responsive [18–20]. Several strategies have been employed to narrow the band gap and broaden the visible light absorption range of these photocatalysts. For example, the $BiOCl_xBr_{1-x}$ [21], $BiOBr_xI_{1-x}$ [22] and $BiOCl_xI_{1-x}$ [23] are prepared to adjust the band gap of the composites, all of which show high photocatalytic activity. Construction of heterostructures via combination of two or three semiconductors

---

* Corresponding authors.
   E-mail addresses: hangui@yzu.edu.cn (G. Han), songxuchunfj@163.com (X.C. Song).

with matching energy band potentials, such as BiOCl/Ag$_3$PO$_4$ [24], BiOCl/BiPO$_4$ [25], BiOBr/Ag$_3$PO$_4$ [26], LaVO$_4$/BiOBr [27], BiOCl/BiOI [28], AgI/BiOI [29] and Pd/BiOCl/BiOI [30] have turned out to be effective strategy for broadening the visible light absorption of catalysts because heterojunction can effectively adjust the electronic properties of composites. Besides, Lin et al have successfully constructed the BiOI/ZnO composite which shows remarkably enhanced photocatalytic activity for the degradation of phenol solution under simulated solar light irradiation [31]. Although the photocatalytic performance of BiOCl/Ag$_3$PO$_4$ and BiOBr/Ag$_3$PO$_4$ heterojunctions have been reported. And to the best of our knowledge, there are no any report on the photodegrading uncolored phenol performance in the Ag$_3$PO$_4$-BiOCl$_{1-x}$Br$_x$.

In this paper, a series of novel heterostructures comprising BiOCl$_{1-x}$Br$_x$ solid solutions and Ag$_3$PO$_4$ was successfully constructed through loading amounts of BiOCl$_{1-x}$Br$_x$ plates onto the surface of Ag$_3$PO$_4$ nanoparticles. The photocatalytic performance for the degradation of phenol solution is also evaluated under simulated solar light irradiation. And the obtained Ag$_3$PO$_4$-BiOCl$_{1-x}$Br$_x$ composites show remarkably enhanced photocatalytic activities for the degradation of the aqueous phenol. After 75 min of simulated solar light irradiation, the photodegradation efficiency of phenol solution is about 97.9% for the Ag$_3$PO$_4$-BiOCl$_{0.75}$Br$_{0.25}$ composites. Furthermore, a probable mechanism toward understanding the phenol photodegradation of the Ag$_3$PO$_4$-BiOCl$_{1-x}$Br$_x$ composites has been proposed and further discussed.

2. Experimental section

2.1. Synthesis

The BiOCl$_{1-x}$Br$_x$ (x = 0, 0.25, 0.5, 0.75, 1) solid solutions were synthesized through a simple precipitation method. First of all, 0.01 mol of Bi(NO$_3$)$_3$·5H$_2$O (4.8508 g) was dissolved in 20 mL ethylene glycol under continuously stirring. Subsequently, stoichiometric amounts of KCl and KBr were dissolved in 20 mL distilled water to obtain a clear solution. Then the solution was added into the previous solution and placed it in 85 ∘C water bath under strongly stirring for 5 h. Finally, the products were separated by centrifugation after cooling to room temperature, washed with deionized water and absolute alcohol several times and then dried at 80 ∘C overnight. The powders were successfully collected as the final products.

For the preparation of Ag$_3$PO$_4$-BiOCl$_{1-x}$Br$_x$ composites, 0.5 g of BiOCl$_{1-x}$Br$_x$ (x = 0, 0.25, 0.5, 0.75, 1) solid solutions was dispersed in 20 ml of deionized water under strongly stirring, and then different quantities of Na$_3$PO$_4$ and AgNO$_3$ were added into the suspension. After magnetically stirring for 30 min at room temperature, the Ag$_3$PO$_4$/BiOCl$_{1-x}$Br$_x$ composites were separated by centrifugation, washed and dried at 80 ∘C overnight. The samples with different Ag$_3$PO$_4$/BiOCl$_{1-x}$Br$_x$ weight ratio of 1:4, 1:5 and 1:6 were synthesized. Finally, the Ag$_3$PO$_4$-BiOCl$_{1-x}$Br$_x$ composites were obtained for use.

For comparison, pure Ag$_3$PO$_4$ photocatalyst was synthesized for comparison. Typically, 5 mmol Na$_3$PO$_4$ was dissolved in 10 ml of deionized water under magnetically stirring. 15 mmol AgNO$_3$ dissolved in 10 ml of distilled water and then added drop by drop into the above solution with vigorously stirring. After stirring for 30 min, the yellow precipitate was collected through centrifugation, washed and dried at 80 ∘C overnight.

2.2. Characterization

The structural property and the phase purity of the obtained products were examined by X-ray diffraction (XRD) using Thermo ARL SCINTAG X'TRA with Cu Ka X-ray source (λ = 1.5406 Å) at 40 mA and 40 kV in the 2θ ranges from 10∘ to 70°. The morphologies and dimensions of the obtained samples were obtained by using SEM (Hitachi S-4700), and the scanning voltage was 15 kV. And energy-dispersive

spectroscopy (EDS, Thermo Noran VANTAG-ESI) was employed to analyze the chemical compositions of as-prepared samples. The UV–vis diffuse reflectance spectra was performed by using a UV–vis spectrophotometer (Lambda 850), and BaSO$_4$ was worked as a reflectance standard. Photoelectrochemical measurements were characterized by an electrochemical work station (CHI-650E, China). Platinum wire and Ag/AgCl were acted as counter and the reference electrodes, severally. An aqueous solution of 0.1 M Na$_2$SO$_4$ was used as electrolyte.

2.3. Photocatalytic experiments

The photocatalytic activity of the obtained products was evaluated by degradation of phenol aqueous solution under simulated solar irradiation. The light source was a 300 W Xe lamp. Typically, 10 mg photocatalyst was added into 50 mL phenol aqueous solution (25 mg/L). Before irradiation, the suspensions were placed in dark and maintained for 0.5 h with constantly magnetic stirring to achieve the adsorption-desorption equilibrium. Subsequently, the suspensions were irradiated and sampled under simulated sunlight. 2 mL of suspension was taken at interval of 15 min, and centrifuged at 7000 rpm for 3 min to remove the photocatalyst particles. The concentration of phenol solution was determined by measuring the main absorption intensity at 269 nm, using a UV759S UV–vis spectrophotometer.

3. Results and discussion

XRD analysis was employed to explore the phase structures of the as-prepared catalysts. The XRD patterns of the BiOCl$_{1-x}$Br$_x$ composites with different amounts of Cl ion are displayed in Fig.1a. The XRD patterns for x = 0 and 1 are identical to the reported for BiOCl (JCPDS No. 06-0249) and BiOBr (JCPDS No. 09-0393), respectively. All samples exhibit sharp diffraction peak, showing high crystallinity. Moreover, it can be obviously observed that BiOCl$_{1-x}$Br$_x$ solid solutions show a perfect transition from BiOCl to BiOBr phase without any other impurity phases. With increasing the Cl composition, the peaks of shift to a larger angle, resulting from that the Cl$^-$ has a smaller ionic radius than Br$^-$ (1.81 vs. 1.96 Å). The successive slightly shift of the XRD patterns can be attributed to the successful formation of BiOCl$_{1-x}$Br$_x$ solid solution. Fig. 1b presents the XRD patterns of Ag$_3$PO$_4$-BiOCl$_{1-x}$Br$_x$ (1:5) composites. It is shown that the XRD pattern of pure Ag$_3$PO$_4$ sample can be indexed to the cubic structure of Ag$_3$PO$_4$ phase (JCPDS No. 06-0505) [7], which is consistent well with previously report. For all these composites, the diffraction peaks which belonging to BiOCl$_{1-x}$Br$_x$ solid solutions also shift to the larger angle with the increasing content of Cl. The phase structures of BiOCl$_{1-x}$Br$_x$ composites does not vary greatly after combining with Ag$_3$PO$_4$, which further demonstrate no chemical reaction happened between BiOCl$_{1-x}$Br$_x$ solid solutions and Ag$_3$PO$_4$. No apparent peaks corresponding to pure Ag$_3$PO$_4$ could be observed, illustrating that the amount of Ag$_3$PO$_4$ sample contained in these composites is low and high dispersion evenly on the surface of BiOCl$_{1-x}$Br$_x$. Respect to the existence of Ag$_3$PO$_4$, it was further proved through the below expanded XRD patterns of Ag$_3$PO$_4$-BiOCl$_{0.75}$Br$_{0.25}$ (1:5) composite in Fig. 1c, which was come from the dotted box of Fig. 1b. In the range of 2θ = 22–31°, the peak at 2θ of 22.8° and 25.5°are indexed to (002) and (101) planes of BiOCl$_{0.75}$Br$_{0.25}$, respectively. And the distinct diffraction peaks (2θ) at 29.3°could be indexed to that of cubic Ag$_3$PO$_4$ and correspond to (200) plane. This result could be inferred that the Ag$_3$PO$_4$-BiOCl$_{1-x}$Br$_x$ composites have been successfully synthesized.

The morphologies of BiOCl$_{0.75}$Br$_{0.25}$, Ag$_3$PO$_4$ and Ag$_3$PO$_4$-BiOCl$_{0.75}$Br$_{0.25}$ (1:5) composites were characterized by using SEM. As shown in Fig. 2a, the pure BiOCl$_{0.75}$Br$_{0.25}$ nanoplates are composed of irregular shaped nanoplates with sizes of 100–400 nm. By contrast, the as-synthesized Ag$_3$PO$_4$ appears quasi-spherical nanoparticles with smooth surfaces (Fig. 2b). As shown in Fig. 2c, with the loading of Ag$_3$PO$_4$, it proves that the Ag$_3$PO$_4$ is precipitated on the BiOCl$_{0.75}$Br$_{0.25}$

weight ratio of Ag, P, O, Bi, Cl and Br were 12.78, 1.19, 7.52, 64.32, 8.13 and 6.06 in Ag_3PO_4-$BiOCl_{0.75}Br_{0.25}$ (1:5) composites. In these composites, it can be clearly seen that the weight ratio of Ag, P, O and Bi elements almost keep invariant, while the weight ratio of Cl and Br are varied as the x increase.

Phenol was degraded in aqueous solution to evaluate the photocatalytic activity of the synthesized composites. The degradation of phenol solution was carried out under simulated solar light irradiation. And the results were shown in Fig. 3(a)–(e), which exhibited the ratio of phenol concentration C and initial phenol concentration C_0 versus the photodegradation time. The decrease of phenol solution concentration in the presence of Ag_3PO_4 under simulated solar light is very small, only about 7.3% in 75 min. The photocatalytic activity can be improved when introducing $BiOCl_{1-x}Br_x$ solid solutions. The Ag_3PO_4-$BiOCl_{1-x}Br_x$ (1:5) composites all display superior photocatalytic activities than individual Ag_3PO_4 and $BiOCl_{1-x}Br_x$ solid solutions (x = 0, 0.25, 0.5, 0.75 and 1). Notably, the phenol degradation efficiency of Ag_3PO_4-$BiOCl_{0.75}Br_{0.25}$ (1:5) composite is obviously enhanced. After 75 min of irradiation under simulated solar light, the photodegradation efficiencies of phenol were 72.4%, 97.9% and 7.3% for $BiOCl_{0.75}Br_{0.25}$, Ag_3PO_4-$BiOCl_{0.75}Br_{0.25}$ (1:5) and Ag_3PO_4 composites, respectively. On the basis of previous experimental results, the reaction kinetics of phenol photodegradation can be matched by the Langmuir–Hinshelwood model, which expressed by the following equation [32]

$$\ln(C/C_0) = kt \tag{1}$$

Where C_0 and C are the phenol solution concentration at t = 0 and t = t. And k is the reaction rate constant. It exhibits that $\ln(C/C_0)$ has a linear function vs. the irradiation time (in Fig. 3f). The phenol degradation rates are calculated to be 0.00775, 0.00835, 0.01043, 0.03239 and 0.00918 min^{-1} for Ag_3PO_4-BiOBr (1:5), Ag_3PO_4-$BiOCl_{0.25}Br_{0.75}$ (1:5), Ag_3PO_4-$BiOCl_{0.5}Br_{0.5}$ (1:5), Ag_3PO_4-$BiOCl_{0.75}Br_{0.25}$ (1:5) and Ag_3PO_4-BiOCl (1:5), respectively. Ag_3PO_4-$BiOCl_{0.75}Br_{0.25}$ (1:5) composite possesses the biggest degradation rate, which demonstrates the optimum ratio of Br and Cl reached in this composite.

The optimal Ag_3PO_4-$BiOCl_{0.75}Br_{0.25}$ photocatalyst was obtained by adjusting the weight ratio of Ag_3PO_4 and $BiOCl_{0.75}Br_{0.25}$. Fig. 4 depicts the photocatalytic experiments on the Ag_3PO_4-$BiOCl_{0.75}Br_{0.25}$ composites with different Ag/Bi weight ratios of 1:4, 1:5 and 1:6. After 75 min of simulated sunlight irradiation, the removal rates of phenol were 83.5%, 97.9% and 72.1% for Ag/Bi weight ratios of 1:4, 1:5 and 1:6, respectively. It is clearly seen that Ag_3PO_4-$BiOCl_{0.75}Br_{0.25}$ (1:5) composite possesses the best photocatalytic activity than pure Ag_3PO_4 and $BiOCl_{0.75}Br_{0.25}$, The result also reveals the amount of Ag_3PO_4 is a vital effect on the photocatalytic performance of Ag_3PO_4-$BiOCl_{0.75}Br_{0.25}$ composite, and the Ag_3PO_4-$BiOCl_{0.75}Br_{0.25}$ composite with optimal Ag/Bi weight ratio is 1:5.

The optical properties of Ag_3PO_4 and $BiOCl_{1-x}Br_x$ (x = 0, 0.25, 0.5, 0.75 and 1) solid solutions were measured by UV–vis DRS, as exhibited in Fig. 5a. It can be clearly observed that the Ag_3PO_4 sample displays photoabsorption in the visible region. Meanwhile, the absorption edge of Ag_3PO_4 sample located at about 530 nm, which is agreed with previously report. As for the absorption edges of the $BiOCl_{1-x}Br_x$ (x = 0, 0.25, 0.5, 0.75 and 1) solid solutions vary between those of BiOCl and BiOBr. And the absorption edges of $BiOCl_{1-x}Br_x$ were gradually red shift as x is increased, which indicated that the decoration of Ag_3PO_4 on the surface of $BiOCl_{1-x}Br_x$ photocatalysts might promote the availability of visible light by adjusting the mole ratio of Cl and Br. For semiconductor materials, the band gap energy can be calculated by the following formula

$$A(h\nu - Eg)^{n/2} = \alpha h\nu \tag{2}$$

Where h, ν, A, α and Eg are Planck constant, light frequency, constant, absorption coefficient and the band gap energy, respectively. And n is decided by the type of transition. If the type of optical transition is

Fig. 1. XRD patterns of (a) $BiOCl_{1-x}Br_x$ solid solutions; (b) Ag_3PO_4-$BiOCl_xBr_{1-x}$ (1:5) composites (x = 0, 0.25, 0.5, 0.75 and 1) (c) the expanded XRD patterns of Ag_3PO_4-$BiOCl_{0.75}Br_{0.25}$ in the range of 2θ = 22–31°.

nanoplates successfully. EDS was used to determine the composition of the composite. Therefore, the Ag_3PO_4-$BiOCl_{0.75}Br_{0.25}$ (1:5) composites were further analyzed by element mapping analysis (Fig. 2d) and EDS analysis (Fig. 2e). The results reveal the presence of O, P, Bi, Cl, Br and Ag elements, suggesting the co-existing of both Ag_3PO_4 and $BiOCl_{0.75}Br_{0.25}$. The weight ratio of Ag_3PO_4-$BiOCl_{1-x}Br_x$ composites from EDS analysis was shown in Table 1. It can be calculated that the

Fig. 2. SEM images of (a) $BiOCl_{0.25}Br_{0.75}$, (b) Ag_3PO_4, (c) Ag_3PO_4-$BiOCl_{0.75}Br_{0.25}$ (1:5), respectively; (d) EDS analysis of Ag_3PO_4-$BiOCl_{0.75}Br_{0.25}$; and (e) EDS mapping of the Ag_3PO_4-$BiOCl_{0.75}Br_{0.25}$ (1:5) composite.

Table 1
The weight ratio of the Ag_3PO_4-$BiOCl_{1-x}Br_x$ composites from EDS analysis.

	Element wt %					
	Ag	P	O	Bi	Cl	Br
Ag_3PO_4-BiOCl (1:5)	12.91	1.24	7.69	66.91	11.25	0
Ag_3PO_4-$BiOCl_{0.75}Br_{0.25}$ (1:5)	12.78	1.19	7.52	64.32	8.13	6.06
Ag_3PO_4- $BiOCl_{0.5}Br_{0.5}$ (1:5)	13.05	1.22	7.31	60.84	5.21	12.37
Ag_3PO_4- $BiOCl_{0.25}Br_{0.75}$ (1:5)	12.84	1.21	7.06	58.76	2.52	17.61
Ag_3PO_4-BiOBr (1:5)	13.16	1.29	6.95	56.42	0	22.18

indirect, the value of n is 4; and the transition is direct, n is1. Fig. 5b shows the plot of $(ahv)^{1/2}$ versus hv. For pure Ag_3PO_4, the band gap is about 2.43 eV, while the band gaps of solid solutions ($BiOBr$, $BiOCl_{0.25}Br_{0.75}$, $BiOCl_{0.5}Br_{0.5}$, $BiOCl_{0.75}Br_{0.25}$ and $BiOCl$) are 2.81, 2.88, 2.97, 3.05 and 3.3 eV, respectively. The result shows that the band gap energy is increased as the content of Cl is increased. The band edge position of CB and VB of semiconductor photocatalysts is an important element for the effective photocatalytic degration of organic contaminants, which can be evaluated by the following equations [33]:

$$E_{CB} = X - E_C - 0.5E_g \tag{3}$$

$$E_{VB} = E_{CB} + E_g \tag{4}$$

Where E_c, X and E_g are the energy of free electrons on the hydrogen scale (4.5 eV), the absolute electronegativity of the semiconductor and the bandgap of the semiconductor, respectively. And E_{VB} and E_{CB} are the valence band edge position and the conduction band edge position. According to these empirical expressions, the calculated data are summarized in Table 2.

The relative valence band edge position and conduction band edge position of $BiOCl_{1-x}Br_x$ (x = 0, 0.25, 0.5, 0.75 and 1) solid solutions are depicted in Fig. 6. It is obviously that the VB edge potential of $BiOCl_{1-x}Br_x$ solid solutions increases gradually from 3.09, 3.16, 3.26, 3.35 to 3.54 eV as x decreases, demonstrating the oxidation ability becomes stronger, while the capability of light absorption becomes weaker. However, the conduction band (CB) edge potential changes in an irregular way. Firstly, it increases from 0.19 eV to 0.30 eV when x increases to 0.25, then drops to 0.29 eV when x = 0.5, at last drops down to 0.28 eV and maintain at it when x = 0.75 and x = 1. Furthermore, it is clearly that Ag_3PO_4 and BiOCl sample has nested band structure, which is unfavorable for the separation of photo-generated carriers in the improvement of photocatalytic performance. While the Ag_3PO_4 and $BiOCl_{1-x}Br_x$ (x = 0.25, 0.5, 0.75 and 1) samples can constitute an interactive band structure, which might be well beneficial to improve the photocatalytic activity. Meanwhile, it is obviously that the energy band positions can be adjusted by changing the content of Cl. It is known to us all that the photocatalytic activities of catalyst

Fig. 3. (a)–(e) The plot of C/C$_0$ vs. the irradiation time of Ag$_3$PO$_4$, Ag$_3$PO$_4$-BiOCl$_{1-x}$Br$_x$ (1:5) and BiOCl$_{1-x}$Br$_x$, respectively; (a) x = 1, (b) x = 0.75, (c) =0.5, (d) =0.25 and (e) =0; (f) Plot of ln (C/C$_0$) against the irradiation time under simulated solar light irradiation over the Ag$_3$PO$_4$-BiOCl$_{1-x}$Br$_x$ (1:5) composites.

depend greatly on the light absorption of incident photons, the energy band configuration which decides the photoexcitation and separation of photo-generated carriers and the redox capability of electrons and holes. Therefore, the photocatalytic activity of Ag$_3$PO$_4$-BiOCl$_{1-x}$Br$_x$ composites could be ascribed to the following reasons. Firstly, the level of VB decreases when x increasing, while the CB edge slightly rises, indicating the band gaps become narrow, which could restrain the redox capability of electrons and holes. Meanwhile, the light absorption capacity becomes stronger as x increasing. And it is notable to find the contradiction between the light absorption and the oxidation ability of electrons and holes. In order to get the balance between these factors, the best strategy is to adjust the energy band configuration and find the excellent photocatalyst. The excellent photocatalytic activity of

Ag$_3$PO$_4$-BiOCl$_{0.75}$Br$_{0.25}$ composite could be ascribed to the appropriate band-gap structure which facilitates the separation of electron-hole pairs and light absorption capacity. As for the Ag$_3$PO$_4$-BiOCl composite, the enhancement of photocatalytic activity might be attributed to the light absorption capacity becomes stronger after loading Ag$_3$PO$_4$ on the surface of BiOCl.

To further identify the discussed above, photocurrent measurements were carried out. It is known that the photocurrent density is connected with the recombination of photogenerated electrons and holes. As shown in Fig. 7a, the photocurrents were measured on Ag$_3$PO$_4$, Ag$_3$PO$_4$-BiOCl$_{0.75}$Br$_{0.25}$ and BiOCl$_{0.75}$Br$_{0.25}$ under the solar light irradiation. As expected, the current is low when the light was turned off and the high photocurrent can be excited under the solar light irradiation. And a

series of identical photocurrent can be identified with good reproducibility when the light is successively light-on and light-off at an interval of 10 s. Comparatively, the Ag_3PO_4-$BiOCl_{0.75}Br_{0.25}$ (1:5) composite shows the highest photocurrent intensity than Ag_3PO_4 and $BiOCl_{0.75}Br_{0.25}$ solid solution. With the decoration of Ag_3PO_4 on the surface of $BiOCl_{0.75}Br_{0.25}$ photocatalyst, the photocurrent intensity was increased, indicating a decrease in recombination probability. The results of photocurrent measurement certify that loading Ag_3PO_4 on the surface of $BiOCl_{0.75}Br_{0.25}$ photocatalyst would facilitate the separation and transfer of photo-generated electron-hole pairs, and decrease the recombination rate of photogenerated charge carriers, leading to superior phenol photodegradation efficiency. On the contrary, Fig. 7b shows the photocurrents of Ag_3PO_4, Ag_3PO_4-BiOCl and BiOCl composites, while the Ag_3PO_4-BiOCl displays the lower photocurrent density than that of BiOCl. It might be related to the nested band structure of Ag_3PO_4 and BiOCl, which is unfavor for the separation of photo-generated carriers. However, the enhanced phenol photodegradation efficiency was achieved for Ag_3PO_4-BiOCl under solar light might due to the enhancement of light absorption.

The radicals and holes trapping measurements were performed to identify the major active species during the photodegradation process. Isopropanol (IPA), benzoquinone (BQ) and ammonium oxalate (AO) were used as effective scavengers to trap hydroxyl radicals ($\cdot OH$), superoxide radicals ($\cdot O_2^-$) and hole (h^+). It can be seen (Fig. 8) that the photocatalytic degradation of phenol molecules is remarkably restrained by the addition of IPA, AO and BQ. As shown in Fig. 8, the degradation efficiency of phenol is significantly decreased from 97.9% to 26.5%, 26.8% and 29.0% when IPA, BQ and AO were severally added into the system through the photocatalytic reaction process. These results demonstrate that $\cdot O_2^-$, h^+ and $\cdot OH$ are all the major active species in the photocatalytic degradation of phenol solution under solar light irradiation.

According to the above experimental results, a probable mechanism for the enhanced photocatalytic decomposition of phenol by the Ag_3PO_4-$BiOCl_{0.75}Br_{0.25}$ composite was depicted in Fig. 9. It is obvious that the redox potentials of CB and VB of $BiOCl_{0.75}Br_{0.25}$ are more positive than those of Ag_3PO_4 and an over-lapping band structure can be formed by Ag_3PO_4 and $BiOCl_{0.75}Br_{0.25}$, which is beneficial for the separation of electron hole pairs. Under simulated solar light irradiation, the electron of $BiOCl_{0.75}Br_{0.25}$ and Ag_3PO_4 can be promoted from the valence band edge to the conduction band, then lead to the formation of electron-hole pairs. Since the CB potential of Ag_3PO_4 (0.25 eV) is more negative than that of $BiOCl_{0.75}Br_{0.25}$ (0.30 eV), the photogenerated electrons on Ag_3PO_4 particle surfaces transfer to $BiOCl_{0.75}Br_{0.25}$ via the well-developed interface. Whereas holes from the valence band of $BiOCl_{0.75}Br_{0.25}$ are injected into the valence band of Ag_3PO_4. The photo-induced electrons on the CB of $BiOCl_{0.75}Br_{0.25}$ would be further captured by oxygen molecules through generating reactive $\cdot O_2^-$ then reacted with the reagent phenol on the surface of the composite. In addition, VB of Ag_3PO_4 (2.68 eV) is more positive than the standard potential OH–/$\cdot OH$ (1.99 eV) [33]. This indicated that the holes in the VB of Ag_3PO_4 directly oxidized H_2O or hydroxide ion (OH–) into $\cdot OH$, then reacts with phenol and effectively decomposes it into other products. It can be concluded that $\cdot O_2^-$ radicals, $\cdot OH$ and h^+ are all the main active species in the degradation of phenol over the Ag_3PO_4-$BiOCl_{0.75}Br_{0.25}$ composite. As a consequence, the separation of the photo-induced electrons and holes on the interface in the Ag_3PO_4-$BiOCl_{0.75}Br_{0.25}$ composite would decrease the recombination rate and improve the photocatalytic performance.

4. Conclusion

In summary, the Ag_3PO_4-$BiOCl_{1-x}Br_x$ composites have been successfully synthesized through a facile two-step synthetic method. The Ag_3PO_4-$BiOCl_{0.75}Br_{0.25}$ (1:5) composite exhibited superior photocatalytic performance, and the phenol photodegradation rate reached
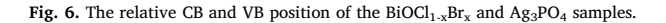
Fig. 4. The plot of C/C_0 versus the irradiation time of Ag_3PO_4, Ag_3PO_4-$BiOCl_{0.75}Br_{0.25}$ (1:4, 1:5 and1:6) and $BiOCl_{0.75}Br_{0.25}$, respectively.

Fig. 5. UV–vis DRS spectrum of the as-prepared (a) Ag_3PO_4 and $BiOCl_{1-x}Br_x$; (b) Plot of the $(\alpha h\nu)^{1/2}$ versus $h\nu$ of $BiOCl_{1-x}Br_x$ and Ag_3PO_4 samples (x = 0, 0.25, 0.5, 0.75, 1).

Table 2
Absolute electronegativity, band gap energy, calculated CB edge and VB edge of as-Prepared $BiOCl_{1-x}Br_x$ and Ag_3PO_4.

	X (eV)	E_g (eV)	E_{VB} (eV)	E_{CB} (eV)
BiOCl	6.36	3.35	3.54	0.19
$BiOCl_{0.75}Br_{0.25}$	6.32	3.05	3.35	0.30
$BiOCl_{0.5}Br_{0.5}$	6.27	2.97	3.26	0.29
$BiOCl_{0.25}Br_{0.75}$	6.22	2.88	3.16	0.28
BiOBr	6.18	2.81	3.09	0.28
Ag_3PO_4	5.96	2.43	2.68	0.25

Fig. 6. The relative CB and VB position of the $BiOCl_{1-x}Br_x$ and Ag_3PO_4 samples.

Fig. 8. Effects of radical scavengers in the degradation process of phenol over Ag_3PO_4-$BiOCl_{0.75}Br_{0.25}$ (1:5).

Fig. 7. (a) Photocurrent responses of the Ag_3PO_4, $BiOCl_{0.75}Br_{0.25}$ and Ag_3PO_4-$BiOCl_{0.75}Br_{0.25}$ (1:5) (b) Photocurrent responses of Ag_3PO_4, $BiOCl$ and Ag_3PO_4-$BiOCl$ (1:5) under solar light irradiation.

97.9% under 75 min of simulated solar light irradiation. The superior photocatalytic activity is derived from the adjustable energy band structure. A reasonable mechanism for prominent photocatalytic activity is discussed by Ag_3PO_4 to promote the charge separation, and to restrain the recombination of photoinduced charge carriers in $BiOCl_{0.75}Br_{0.25}$ efficiently. More importantly, the light absorption range can be extended by loading Ag_3PO_4, which facilitates the phenol degradation activity. The results indicate that Ag_3PO_4-$BiOCl_{0.75}Br_{0.25}$ photocatalyst might be a promising material in practical applications in future.

Fig. 9. Schematic illustration of the photocatalysis process over Ag_3PO_4-$BiOCl_{0.75}Br_{0.25}$ (1:5) composite.

References

[1] D.Z. Lu, M.C. Yang, P.F. Fang, C.H. Li, L.L. Jiang, Enhanced photocatalytic degradation of aqueous phenol and Cr(VI) over visible-light-driven Tb_xO_y loaded TiO_2-oriented nanosheets, Appl. Surf. Sci. 399 (2017) 167–184.

[2] Z. Wei, F.F. Liang, Y.F. Liu, W.J. Luo, J. Wang, W.Q. Yao, Y.F. Zhu, Photoelectrocatalytic degradation of phenol-containing wastewater by TiO_2/g-C_3N_4 hybrid heterostructure thin film, Appl. Catal. B: Environ. 201 (2017) 600–606.

[3] M.C. Long, W.M. Cai, J. Cai, B.X. Zhou, X.Y. Chai, Y.H. Wu, Efficient photocatalytic degradation of phenol over $Co_3O_4/BiVO_4$ composite under visible light irradiation, J. Phys. Chem. B 110 (2006) 20211–20216.

[4] J.H. Yao, H. Chen, F. Jiang, Z.Y. Jiao, M.C. Jin, Titanium dioxide and cadmium sulfide co-sensitized graphitic carbon nitride nanosheets composite photocatalysts with superior performance in phenol degradation under visible-light irradiation, J. Colloid Interface Sci. 490 (2017) 154–162.

[5] R.P. Li, X.H. Song, Y.P. Huang, Y.F. Fang, M.K. Jia, W.H. Ma, Visible-light photocatalytic degradation of azo dyes in water by Ag$_3$PO$_4$: an unusual dependency between adsorption and the degradation rate on pH value, J. Mol. Catal. A: Chem. 421 (2016) 57–65.

[6] R. Jiang, H.Y. Zhu, J.B. Li, F.Q. Fu, J. Yao, X.X. Liang, R.Q. Guo, G.M. Zeng, Eficient solar photocatalyst based on Ag$_3$PO$_4$/graphene nanosheets composite for photocatalytic decolorization of dye pollutants, J. Iran. Chem. Soc. 13 (2016) 1167–1174.

[7] Y. Li, P.F. Wang, C.P. Huang, W.F. Yao, Q. Wu, Q.J. Xu, Synthesis and photocatalytic activity of ultrafine Ag$_3$PO$_4$ nanoparticles on oxygen vacated TiO$_2$, Appl. Catal. B: Environ. 205 (2017) 489–497.

[8] P.F. Tan, X. Chen, L.D. Wu, Y.Y. Shang, W.W. Liu, J. Pan, X. Xiong, Hierarchical flower-like SnSe$_2$ supported Ag$_3$PO$_4$ nanoparticles: towards visible light driven photocatalyst with enhanced performance, Appl. Catal. B: Environ. 202 (2017) 326–334.

[9] Z. Cui, Y. Sun, Z. Zhang, M. Xu, B. Xin, Facile synthesis and photocatalytic activity of Ag$_3$PO$_4$ decorated MoS$_2$ nanoflakes on carbon fiber cloth, Mater. Res. Bull. 100 (2018) 345–352.

[10] N. Mohaghegh, E. Rahimi, BiPO$_4$ photocatalyst employing synergistic action of Ag/Ag3PO4 nanostructure and graphene nanosheets, Solid State Sci. 56 (2016) 10–15.

[11] Y. Chang, K. Yu, C.X. Zhang, R. Li, P.Y. Zhao, L.L. Lou, S.X. Liu, Three-dimensionally ordered macroporous WO$_3$ supported Ag$_3$PO$_4$ with enhanced photocatalytic activity and durability, Appl. Catal. B: Environ. 176 (2015) 363–373.

[12] J.Q. Zhang, K. Yu, Y.F. Yu, L.L. Lou, Z.Q. Yang, J.W. Yang, Highly effective and stable Ag$_3$PO$_4$/WO$_3$ photocatalysts for visible light degradation of organic dyes, J. Mol. Catal. A: Chem. 391 (2014) 12–18.

[13] Q.S. Yan, M.M. Xu, C.P. Lin, J.F. Hu, Y.G. Liu, R.Q. Zhang, Efficient photocatalytic degradation of tetracycline hydrochloride by Ag$_3$PO$_4$ under visible-light irradiation, Environ. Sci. Pollut. Res. 23 (2016) 14422–14430.

[14] H.F. Cheng, B.B. Huang, Y. Dai, Engineering BiOX (X = Cl, Br, I) nanostructures for highly efficient photocatalytic applications, Nanoscale 6 (2014) 2009–2026.

[15] D. Zhang, J. Li, Q.G. Wang, Q.S. Wu, High {001} facets dominated BiOBr lamellas: facile hydrolysis preparation and selective visible-light photocatalytic activity, J. Mater. Chem. A 1 (2013) 8622–8629.

[16] K. Zhang, D. Zhang, J. Liu, K. Ren, H. Luo, Y. Peng, G. Li, X. Yu, A novel nanoreactor framework of iodine-incorporated BiOCl core-shell structure: enhanced light-harvesting system for photocatalysis, CrystEngComm 14 (2012) 700–707.

[17] O. Mehraj, N.A. Mir, B.M. Pirzada, S. Sabir, Fabrication of novel Ag$_3$PO$_4$/BiOBr heterojunction with high stability and enhanced visible-light-driven photocatalytic activity, Appl. Surf. Sci. 332 (2015) 419–429.

[18] Y. Xu, X. Hu, H. Zhu, J. Zhang, Insights into BiOCl with tunable nanostructures and their photocatalytic and electrochemical activities, J. Mater. Sci. 51 (2016) 4342–4348.

[19] J. Song, Q. Fan, W. Zhu, R. Wang, Z. Dong, Preparation of BiOCl with high specific surface area and excellent visible light photocatalytic activity, Mater. Lett. 165 (2016) 14–18.

[20] J. Yuan, J. Wang, Y. She, J. Hu, P. Tao, F. Lv, Z. Lu, Y. Gu, BiOCl micro-assembles consisting of ultrafine nanoplates: a high peformance electro-catalyst for air electrode of Al–air batteries, J. Power Sources 263 (2014) 37–45.

[21] X.M. Mao, C.M. Fan, Effect of light response on the photocatalytic activity of BiOCl$_x$Br$_{1-x}$ in the removal of rhodamine B from water, Int. J. Miner. Metall. Mater. 20 (2013) 1089–1095.

[22] Z.F. Jia, F.M. Wang, F. Xin, B.Q. Zhang, Simple solvothermal routes to synthesize 3D BiOBr$_x$I$_{1-x}$ microspheres and their visible-light-induced photocatalytic properties, Ind. Eng. Chem. Res. 50 (2011) 6688–6694.

[23] W.J. Kim, D. Pradhan, B.K. Min, Adsorption/photocatalytic activity and fundamental natures of BiOCl and BiOCl$_x$I$_{1-x}$ prepared in water and ethylene glycol environments, and Ag and Au-doping effects, Appl. Catal. B: Environ. 147 (2014) 711–725.

[24] B.C. Cao, P.Y. Dong, S. Cao, Y.H. Wang, BiOCl/Ag$_3$PO$_4$ composites with highly enhanced ultraviolet and visible light photocatalytic performances, J. Am. Ceram. Soc. 96 (2013) 544–548.

[25] Y. Hu, Z. Jia, R. Lv, C. Fan, H. Zhang, One-pot electrochemical preparation of BiOCl/BiPO4 double-layer heterojunction film with efficientphotocatalytic performance, Mater. Res. Bull. 94 (2017) 222–230.

[26] Z.K. Cui, F.L. Zhang, Z. Zheng, W.J. Fa, B.J. Huang, Preparation and characterisation of Ag$_3$PO$_4$/BiOBr composites with enhanced visible light driven photocatalytic performance, Mater. Technol. 29 (2014) 214–219.

[27] J. Ma, S. Liu, G. Qi, Synthesis of m-LaVO$_4$/BiOBr composite photocatalysts and their photocatalytic performance under visible light, Mater. Res. Bull. 95 (2017) 146–151.

[28] H.W. Huang, X. Han, X.W. Li, S.C. Wang, P.K. Chu, Y.H. Zhang, Multiple heterojunctions fabrication with tunable visible-light-active photocatalytic reactivity in the BiOBr-BiOI full range composites based on microstructure modulation and band structures, ACS Appl. Mater. Interfaces 7 (2015) 482–492.

[29] M.J. Islam, D.A. Reddy, R. Ma, Y.J. Kim, T.K. Kim, Reduced-graphene-oxide-wrapped BiOI-AgI heterostructured nanocomposite as a high-performance photocatalyst for dye degradation under solar light irradiation, Solid State Sci. 61 (2016) 32–39.

[30] L.Z. Ren, D.E. Zhang, X.Y. Hao, X. Xiao, Z.W. Tong, Facile synthesis of flower-like Pd/BiOCl/BiOI composites and photocatalytic properties, Mater. Res. Bull. 94 (2017) 183–189.

[31] J.J. Jiang, H.T. Wang, X.D. Chen, S. Li, T.F. Xie, D.J. Wang, Y.H. Lin, Enhanced photocatalytic degradation of phenol and photogenerated charges transfer property over BiOI-loaded ZnO composites, J. Colloid Interface Sci. 494 (2017) 130–138.

[32] X. Cui, Y.F. Zheng, H. Zhou, H.Y. Yin, X.C. Song, The effect of synthesis temperature on the morphologies and visible light photocatalytic performance of Ag$_3$PO$_4$, J. Taiwan Inst. Chem. Eng. 60 (2016) 328–334.

[33] Q.W. Cao, Y.F. Zheng, X.C. Song, The enhanced visible light photocatalytic activity of Bi$_2$W$_x$Mo$_{1-x}$O$_6$-BiOCl heterojunctions with adjustable energy band, Ceram. Int. 42 (2016) 14533–14542.